Adsorption (2013) 19:11–23
DOI 10.1007/s10450-012-9406-2

Carbon monoxide isotope enrichment and separation by pressure swing adsorption

Shubhra J. Bhadra · Armin D. Ebner · James A. Ritter

Received: 26 March 2012 / Accepted: 20 August 2012 / Published online: 5 September 2012

Abstract Simulations of three different 3-bed 3-step pressure swing adsorption (PSA) cycles were carried out to study the enrichment and recovery of ^{14}CO from an isotopic mixture of ^{14}CO, ^{13}CO and ^{12}CO using NaX zeolite. Each PSA cycle included feed pressurization/feed (FP/P), heavy reflux (HR) and countercurrent depressurization (CnD) steps; they differed only in the way the CnD step was carried out: PSA Cycle I was carried out under total reflux (i.e., with no ^{14}CO heavy product production); PSA Cycle II was carried out with discontinuous ^{14}CO heavy product production; and PSA Cycle III was carried out with continuous ^{14}CO heavy product production. The effects of the CnD step valve coefficient (c_v), heavy reflux ratio (R_R), and cycle time (t_{cyc}) on the PSA process performance were determined in terms of the ^{14}CO enrichment, ^{14}CO recovery and CO feed throughput. The results showed that there was essentially no limit to the extent of the ^{14}CO enrichment, despite the inherently low ^{14}CO/^{12}CO (1.05) and ^{14}CO/^{13}CO (1.12) separation factors for these isotopes on NaX zeolite. Under total reflux an optimum c_v was found for the CnD step and ^{14}CO enrichments as high as 152 were obtained. Using the optimum c_v under finite reflux, a ^{14}CO enrichment approaching 20 and a ^{14}CO recovery approaching 100 % were easily achieved with discontinuous (PSA Cycle II) or continuous (PSA Cycle III) ^{14}CO heavy product production. There was essentially no difference in the performance of PSA Cycles II and III, a counterintuitive result. The ^{14}CO enrichment and the ^{14}CO recovery both increased with decreasing CO feed throughputs and higher R_R, which were always very close to unity.

S.J. Bhadra · A.D. Ebner · J.A. Ritter (✉)
Department of Chemical Engineering, University of South Carolina, Columbia, SC 29208, USA
e-mail: ritter@cec.sc.edu

Keywords Isotope separation · PSA · Pressure swing adsorption · Carbon isotope separation · Nuclear waste

Nomenclature

B_i	parameter in Eq. (8), K
b_i	Toth isotherm parameter in Eq. (7), kPa^{-1}
b_i^0	parameter in Eq. (8), kPa^{-1}
$C_{p,a,i}$	heat capacity of component i in the adsorbed phase, kJ/mol/K
$C_{p,g,i}$	heat capacity of component i in the gas phase, kJ/mol/K
$C_{p,p}$	heat capacity of the particle, kJ/mol/K
c_v	valve coefficient, dimensionless in unit specific Eq. (14)
F	flow rate, SLPM
h_w	overall heat transfer coefficient, kW/m^2/K
ΔH_i	isosteric heat of adsorption of component i, kJ/mol
k_i	LDF mass transfer coefficient of component i, s^{-1}
L	length of the column, m
M_g	average molecular weight of the gas phase, mol/kg
n_j	Toth isotherm parameter in Eq. (7)
$n_{t,i}$	parameter in Eq. (9)
$n_{o,i}$	parameter in Eq. (9)
N	number of components
P	pressure, kPa
P_H	high pressure, kPa
P_L	low pressure, kPa
P_o	pressure downstream of the valve, kPa
q_i	amount adsorbed of component i, mol/kg
q_i^s	Toth isotherm parameter in Eq. (7), mol/kg
q_i^*	equilibrium amount adsorbed of component i, mol/kg
$q_{o,i}^s$	parameter in Eq. (10), mol/kg
$q_{t,i}^s$	parameter in Eq. (10), mol/kg/K
R	universal gas constant, kPa m^3/mol/K

r_b radius of the column, m
r_p radius of the particle, m
R_R reflux ratio
S_g specific gravity
t time, s
t_{cyc} cycle time, s
T temperature, K
T_F feed temperature, K
T_o ambient temperature, K
v interstitial velocity, m/s
y_i mole fraction of component i
z axial coordinate in the bed, m

Greek Symbols

ε_b bed porosity
ε_p particle porosity
μ_g viscosity of the gas phase, kg/m/s
ρ_p particle density, kg/m^3

1 Introduction

The impetus for this work stemmed from the world-wide stockpiling of 250,000 tons of spent graphite rods from nuclear reactors (Fachinger et al. 2008). The graphite used in many nuclear reactors undergoes transmutation, transforming some of the ^{12}C into ^{14}C, a long-lived radioactive isotope. This process contaminates the graphite with about 1 ppm of ^{14}C, i.e., about one million times its natural abundance (Izumi et al. 2005; Fachinger et al. 2008).

To avoid storing all of this spent graphite as a high-level radioactive waste for hundreds of years, it has been proposed to gasify all of it into CO or CO_2, separate the gaseous ^{14}C isotope from the other gaseous carbon isotopes, release the substantially decontaminated gas into the environment and store the concentrated ^{14}C in a solid after conversion to carbon black or some other carbon-containing solid (Izumi et al. 2005; Fachinger et al. 2008). In this way, the percent recovery of ^{14}C from the graphite would correspond to the same percent reduction in waste volume (relative to graphite). It is worth pointing out that this is a gargantuan waste treatment issue that may take many decades to complete at a very high cost, no matter the isotope separation process.

Izumi et al. (2005) proposed a 3-bed 3-step PSA process for carbon isotope separation in the form of CO. CO was most likely selected over CO_2 because of the molecular weight advantage associated with the former when considering adsorption. They carried out an experimental study to determine the equilibrium constants of ^{12}CO, ^{13}CO and ^{14}CO and temperature dependence of the ^{13}CO/^{12}CO and ^{14}CO/^{12}CO separation factors on NaX zeolite. A maximum separation factor of 1.08 was obtained for ^{14}CO/^{12}CO at 243 K, whereas a maximum separation factor of 1.10 was obtained for ^{13}CO/^{12}CO at 213 K. Hence, the adsorption capacity of these CO isotopes on NaX zeolite decreases as: ^{14}CO > ^{13}CO > ^{12}CO. Using the proposed 3-bed 3-step PSA cycle and NaX zeolite they attained a ^{14}CO enrichment of about 2.5 at 213 K. However, the ^{14}CO enrichment was the only PSA performance indicator reported. Nothing was mentioned about the ^{14}CO recovery and CO feed throughput of the PSA process.

Therefore, the objective of this feasibility study was to investigate via process simulation the overall performance of the 3-bed 3-step PSA cycle proposed by Izumi et al. (2005) for CO isotope separation using NaX zeolite. Three different variants of the 3-bed 3-step PSA process were investigated: (I) the Izumi et al. (2005) cycle under total reflux (i.e., with no heavy ^{14}CO product production), (II) the Izumi et al. (2005) cycle with discontinuous heavy ^{14}CO product production based on a concept proposed by Yamaho et al. (1987) for enriching dilute feed streams, and (III) the Izumi et al. (2005) cycle with continuous heavy ^{14}CO product production as presumably used by them. Numerous simulations were carried out to the periodic state using the dynamic adsorption process simulator (DAPS) developed by Ritter and co-workers (Reynolds et al. 2006) using a feed stream consisting of only CO isotopes. A wide range of valve coefficients, reflux ratios and cycle times were investigated and the corresponding ^{14}CO enrichments, ^{14}CO recoveries and CO feed throughputs were determined.

2 PSA cycle descriptions

Figure 1 shows the 3-bed 3-step PSA process proposed by Izumi et al. (2005) (Mode B) and two variants thereof (either Mode A or a combination of Modes A and B, as explained below). The first variant (PSA Cycle I) was operated under total heavy reflux, with no ^{14}CO heavy product production during the cycle. This case represented the best possible ^{14}CO enrichment for a given set of process conditions, just like in distillation. The second variant (PSA Cycle II) was operated with discontinuous ^{14}CO heavy product production during the cycle. This cycle was based on a concept proposed by Yamaho et al. (1987) for enriching dilute adsorbates; its operation is explained in detail below. The third variant (PSA Cycle III) was operated with continuous ^{14}CO heavy product production during the cycle. This variant was presumably the way Izumi et al. (2005) operated the PSA process in their study.

Notice that the three cycle step schedules shown in Fig. 1 are all the same, with each comprising three cycle steps: a feed pressurization/feed (FP/F) step, a heavy reflux (HR) step and a countercurrent depressurization (CnD) step. Each step has the same time duration. A bed undergoing the FP/F

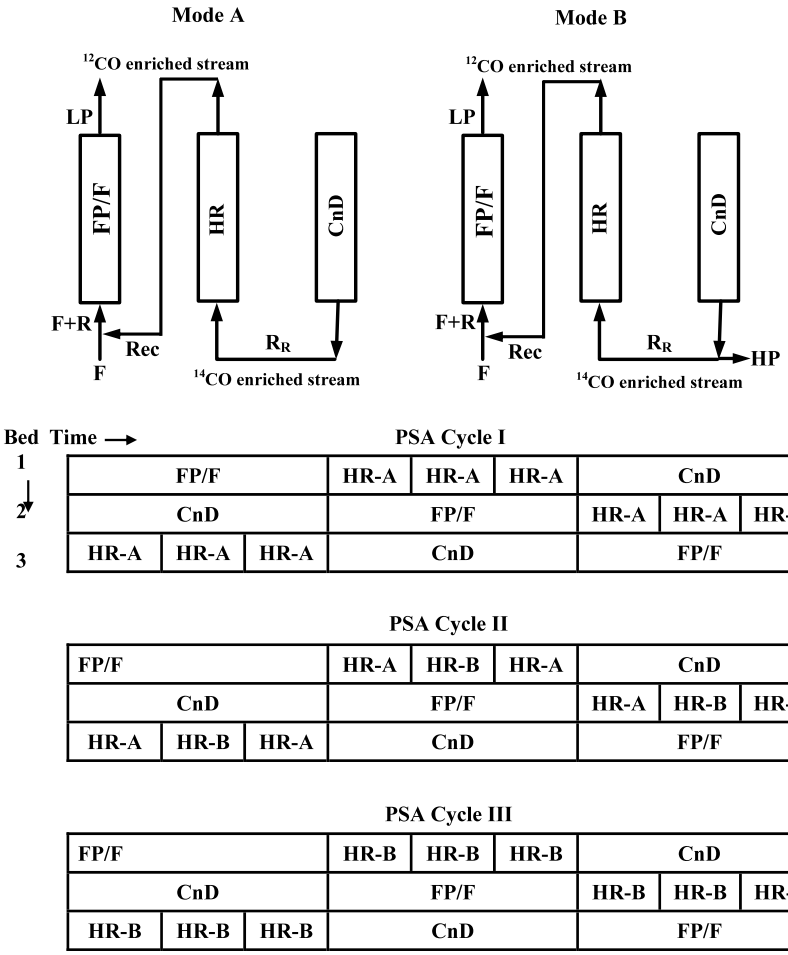

Fig. 1 Diagrams and cycle step schedules for the 3-bed 3-step PSA cycles. *Mode A*: total heavy reflux with no ^{14}CO production. *Mode B*: partial heavy reflux with ^{14}CO production. *PSA Cycle I*: total heavy reflux. *PSA Cycle II*: discontinuous ^{14}CO production. *PSA Cycle III*: continuous ^{14}CO production. FP/F = feed pressurization step, HR-A = heavy reflux step under total heavy reflux ($R_R = 1$), HR-B = heavy reflux step under partial heavy reflux ($R_R < 1$) and CnD = countercurrent depressurization

step is pressurized from a low pressure to a high pressure by feeding a gas stream into the heavy product end of the bed while keeping the light product end of the bed closed. This gas stream is a blend of fresh feed (F) and recycled (Rec) light product from the HR step, as shown. Upon reaching the high pressure, the light product end of the bed is opened and the FP/F step continues by allowing gas to flow through the bed and produce light product (LP).

During the FP/F step the most strongly adsorbed component (i.e., ^{14}CO) is collected in the bed, principally at the feed end, while a stream enriched with the more weakly adsorbed components (i.e., ^{12}CO and ^{13}CO) leaves the light product end of the bed and is collected as the LP. During the HR step, the gas stream enriched with ^{14}CO exiting the heavy product end of the bed undergoing the CnD step is compressed up to the high pressure and either fed cocurrently to the bed undergoing the HR step, withdrawn as the HP or both, as explained below. The purpose of the HR step is to force the weakly adsorbed components to migrate towards the light product end of the bed while increasing the adsorbed phase loading of ^{14}CO near the heavy product end of the bed, which, in turn, increases its enrichment during the subsequent CnD step. The LP exiting the bed undergoing the HR step is completely recycled (Rec) to the bed undergoing the FP/F step by blending it with F, as mentioned above.

During the CnD step, the pressure in the corresponding bed changes from the high pressure to the low pressure by allowing gas to flow countercurrently out of the heavy product end of the bed while keeping the light product end of the bed closed. During this step the ^{14}CO that was adsorbed during the previous two steps and retained nearer the heavy product end of the bed is released from the adsorbent and exits the bed at a higher concentration than in the fresh feed F. Hence, the CnD step is a regeneration step, the only regeneration step in the cycle schedule. The three PSA cycle variants differ from each other only in the way the CnD step is operated.

PSA Cycle I operates under total heavy reflux. In this variant, no HP is ever produced during the CnD step and all the gas exiting the bed undergoing the CnD step is sent to the bed undergoing the HR step. PSA Cycle III operates with continuous HP production. It does this by continuously taking a small fraction of the gas leaving the bed undergoing the CnD step as HP product, while continuously sending the remaining fraction to the bed undergoing the HR

step, as shown in Fig. 1. The reflux ratio (R_R) is defined as the amount of gas sent to the bed undergoing the HR step divided by the total amount of gas exiting the bed during the CnD step. PSA Cycle II operates with discontinuous HP production. It does this by producing HP at a specified R_R only during a fraction of the time the CnD step is operated, just like in PSA Cycle III. During the remaining time, the CnD step is operated under total reflux, just like in PSA Cycle I. PSA Cycle II warrants additional explanation.

Based on concepts introduced by Yamaho et al. (1987) the CnD step is divided into initial, middle and final stages. HP is withdrawn from the bed only during the middle stage of the CnD step because this is where the concentration of the heavy component, in this case ^{14}CO, at some point goes through a maximum. Typically, systems that deal with dilute heavy species exhibit significant changes of concentration (and hence enrichments) of this species during the CnD step, with the transient effluent concentration profile exiting the bed exhibiting a bell-shaped curve. During the initial stage of the CnD step the gas stream leaving the bed is not very enriched in the heavy species because the initial gas exiting the bed consists mostly of gas phase species with a concentration similar to the last bit of gas fed to the bed during the HR step. Similarly, during the final stage of the CnD step the gas stream leaving the bed is also not very enriched in the heavy species, as most of the heavy gas, which was located in the adsorbed phase at the heavy product end of the bed, is no longer present in the bed and has been replaced with the lighter gas coming from regions in the bed more towards the light product end. Hence, between these two stages the concentration of the heavy component goes through a maximum as it exits the bed. The beginning and end points (and thus the duration) of the middle stage during the CnD step is determined by observing when the concentration begins to rise, goes through a maximum and then falls off. HP is withdrawn from the bed only during this middle stage while operating at some finite but large R_R, and the initial and final stages are operated under total reflux, as shown in Fig. 1.

The performance indicators of the PSA cycles are evaluated in terms of ^{14}CO enrichment, ^{14}CO recovery and CO feed throughput, which are defined as:

$$\text{Enrichment} = \frac{\frac{\text{moles}^{14}\text{CO obtained as product during CnD step}}{\text{total moles CO obtained as product during CnD step}}}{^{14}\text{CO mole fraction in fresh feed}} \tag{1}$$

$$\text{Recovery} = \frac{\text{moles}^{14}\text{CO obtained as product during CnD step}}{\text{moles}^{14}\text{CO fed as fresh feed in FP/F step}} \tag{2}$$

$$\text{CO Feed Throughput} = \frac{\text{total moles CO fed as fresh feed in FP/F step}}{(\text{mass adsorbent in one bed})(\text{total cycle time})} \tag{3}$$

3 Dynamic Adsorption Process Simulator (DAPS)

Simulations of the PSA cycles were carried out using the in-house developed DAPS (Reynolds et al. 2006). The following assumptions were imposed: ideal gas behavior, plug flow, no axial dispersion, no film mass transfer resistance (i.e., identical concentrations in both the bulk gas and within the pores of the pellet), linear driving force (LDF) mass transfer resistance between the gas and adsorbed phases, no heat transfer resistance between the gas and solid (i.e., pellet) phases, no thermal capacitance of the wall, and no axial thermal conduction.

For an N-component PSA process, the overall and component differential mass balances are written as

$$\left(\varepsilon_b + (1-\varepsilon_b)\varepsilon_P\right)\frac{P}{RT}\left(\frac{1}{P}\frac{\partial P}{\partial t} - \frac{1}{T}\frac{\partial T}{\partial t}\right) + \frac{\varepsilon_b}{RT}\frac{\partial (vP)}{\partial z} + \sum_{j=1}^{n} S_j = 0 \tag{4}$$

$$\left(\varepsilon_b + (1-\varepsilon_b)\varepsilon_P\right)\frac{P}{RT}\frac{\partial y_i}{\partial t} + \frac{\varepsilon_b v P}{RT}\frac{\partial y_i}{\partial z} - y_i\sum_{j=1}^{n} S_j + S_i = 0 \quad i = 1 \text{ to } N-1 \tag{5a}$$

$$y_i + \sum_{j=1, j\neq i}^{n} y_j = 0 \quad i = N \tag{5b}$$

where $S_i = (1-\varepsilon_b)\rho_p(dq_i/dt)$, and ε_p and ρ_p are the pellet porosity and density, respectively, ε_b is the bed porosity, v is the interstitial velocity, y_i is the mole fraction of species i in the gas phase, T is the temperature of both the gas and solid phases, P is the pressure, R is the universal gas constant, and q_i is the amount adsorbed of species i.

The mass transfer of component i between the gas and adsorbed phases is defined in terms of the linear driving force (LDF) approximation as

$$\frac{\partial q_i}{\partial t} = k_i\left(q_i^* - q_i\right) \quad i = 1 \text{ to } N \tag{6}$$

where k_i is the mass transfer coefficient of component i, assumed to be independent of T and P and the same for each component i. The equilibrium amount adsorbed of component i, q_i^*, was calculated from the mixed-gas Toth isotherm (Jaroniec and Toth 1976) as

$$q_i^* = q_i^s \frac{b_i P y_i}{[1 + (\sum_{j=1}^{N} b_j P y_j)^{n_i}]^{\frac{1}{n_i}}} \tag{7}$$

with the temperature dependences of the parameters, b_i, q_i^s and n_i, given by

$$b_i = b_i^o \exp\left(\frac{B_i}{T}\right) \tag{8}$$

Table 1 Initial and boundary conditions for the 3-bed 3-step PSA cycles shown in Fig. 1[a]

Condition	Cycle step		
	Feed Pressurization/Feed (FP/F)	Heavy Reflux (HR)	Countercurrent Depressurization (CnD)
at $t = 0$ and for $0 \le z/L \le 1$ at end of the previous step	$y_i = y_{i,CnD}$	$y_i = y_{i,FP/F}$	$y_i = y_{i,HR}$
	$v = v_{CnD}$	$v = v_{FP/F}$	$v = v_{HR}$
	$q_i = q_{i,CnD}$	$q_i = q_{i,FP/F}$	$q_i = q_{i,HR}$
	$T = T_{CnD}$	$T = T_{FP/F}$	$T = T_{HR}$
	$P = P_{CnD}$	$P = P_{FP/F}$	$P = P_{HR}$
at $z/L = 0$[b] and for $t_{cs,b} \le t \le t_{cs,e}$	$y_i = [y_{i,F} F_F + y_{i,HR,z/L=1} F_{HR,z/L=1}]/F$	$y_i = y_{i,CnD,z/L=0}$	CMB
	$F = F_F + F_{HR,z/L=1}$	$F = -R_R F_{CnD,z/L=0}$	OMB
	LDFE	LDFE	LDFE
	$T = T_F$	$T = T_F$	EB
	MB	MB	VE ($P_o = P_L, c_v > 0$)
at $z/L = 1$[b] and for $t_{cs,b} \le t \le t_{cs,e}$	CMB	CMB	CMB
	OMB	OMB	VE ($P_o = P_L, c_v = 0$)
	LDFE	LDFE	LDFE
	EB	EB	EB
	VE ($P_o = P_H, c_v > 0$)	VE ($P_o = P_H, c_v > 0$)	MB

[a]Notation: CMB: component mass balance, Eqs. (5a), (5b); OMB: overall mass balance, Eq. (4); LDFE: linear driving force equation, Eq. (6); EB: energy balance, Eq. (11); MB: momentum balance, Eq. (13); VE: valve equation, Eq. (14); F: molar flow rate; P_o: Pressure outside the valve; P_L: low pressure; P_H: high pressure; R_R: heavy reflux ratio

[b]The molar flow rate F is positive with gas flowing towards $z/L = 1$ and negative with gas flowing towards $z/L = 0$. $t_{cs,b}$ and $t_{cs,e}$ are the times at the beginning and end of a cycle step, respectively

$$n_i = \frac{n_{t,i}}{T} + n_{o,i} \tag{9}$$

$$q_i^s = q_{t,i}^s T + q_{o,i}^s \tag{10}$$

The energy balance is written as

$$\begin{aligned}&\left(\varepsilon_b + (1-\varepsilon_b)\varepsilon_P\right)\left(Cp_g \frac{P}{RT}\frac{\partial T}{\partial t} - \frac{\partial P}{\partial t}\right)\\ &\quad + \left((1-\varepsilon_b)\rho_P Cp_p\right)\frac{\partial T}{\partial t} + \varepsilon_b Cp_g v \frac{P}{RT}\frac{\partial T}{\partial z}\\ &\quad + (1-\varepsilon_b)\rho_P \sum_{j=1}^{n}\left(Cp_{a,j} q_j \frac{\partial T}{\partial t} + \Delta H_j \frac{\partial q_j}{\partial t}\right)\\ &\quad + \frac{2}{r_{b,i}} h_w (T - T_o) = 0\end{aligned} \tag{11}$$

with

$$Cp_g = \sum_{j=1}^{n} (y_j Cp_{g,j}) \tag{12}$$

where $Cp_{g,j}$ and $Cp_{a,j}$ are the molar heat capacities of species j in the gas and adsorbed phases, respectively and assumed to be equal, Cp_p is the heat capacity of the pellet, ΔH_i is the isosteric heat of adsorption of species i, h_w is the overall heat transfer coefficient between the wall of the bed and the surroundings outside the bed at ambient temperature T_o, and r_i is the internal radius of the bed.

The pressure drop along the bed was evaluated from the Ergun equation as

$$\begin{aligned}&\frac{\partial P}{\partial z} + 1.5 \times 10^{-1} \mu_g \left(\frac{1-\varepsilon_p}{2 r_p \varepsilon_p}\right)^2 v\\ &\quad + 1.75 \times 10^{-3} M_g \frac{P}{RT}\frac{1-\varepsilon_p}{2 r_p \varepsilon_p} v|v| = 0\end{aligned} \tag{13}$$

where μ_g is the viscosity of the gas phase, M_g is the average molecular weight of the gas phase, and r_p is the effective radius of the pellet.

The equations described above constitute a complete mathematical model for a multi-component PSA process once the initial and boundary conditions for each cycle step are specified. The initial and boundary conditions are summarized in Table 1, which represent the equations used in the first ($z/L = 0$) and last ($z/L = 1$) nodes of the bed with L being the bed length. For each cycle step the initial condition in the bed was taken as that at the end of the previous cycle step. Also, at a bed boundary, when a molar flow rate (F) passes through a valve it is described by the following

Table 2 Bed, adsorbent and process characteristics, and equilibrium and kinetic information used as input to the dynamic adsorption process simulator (DAPS)

Bed characteristics	
Bed radius (m)	0.025
Bed length (m)	0.75
Bed porosity	0.32
Bulk density (kg/m^3)	690.2
Heat transfer coefficient (kW/m^2/K)	0.0067
Adsorbent characteristics	
Adsorbent	NaX Zeolite
Pellet radius (m)	0.0008
Pellet density (kg/m^3)	1015.0
Pellet porosity	0.39
Pellet heat capacity (J/kg/K)	920.0
Process characteristics	
Feed mole fraction: ^{12}CO, ^{13}CO and ^{14}CO	0.980009, 0.01999, 0.000001
Feed temperature (K)	227.59
Ambient temperature (K)	227.59
High pressure (kPa)	120.0
Low pressure (kPa)	1.0
Equilibrium and kinetic information	
Heat of adsorption (kJ/mol)	13.95
B_i for ^{14}CO, ^{13}CO and ^{12}CO (K)	85.5, 85.5, 85.5
b_i^0 for ^{14}CO, ^{13}CO and ^{12}CO (kPa^{-1})	0.0305, 0.0280, 0.0273
$q_{t,i}^s$ for ^{14}CO, ^{13}CO and ^{12}CO (mol/kg/K)	−0.03, −0.03, −0.03
$q_{0,i}^s$ for ^{14}CO, ^{13}CO and ^{12}CO (mol/kg)	9.91, 9.91, 9.91
$n_{t,i}$ for ^{14}CO, ^{13}CO and ^{12}CO (K)	260.9, 260.9, 260.9
$n_{0,i}$ for ^{14}CO, ^{13}CO and ^{12}CO	−0.43, −0.43, −0.43
k_i for ^{14}CO, ^{13}CO and ^{12}CO (s^{-1})	1.0, 1.0, 1.0

valve equation:

$$F = c_v v \frac{1}{\sqrt{S_g T}} \min\left(49.08\left|P^2 - P_o^2\right|^{0.5}, 41.63 P_o\right) \qquad (14)$$

where c_v is the valve coefficient, S_g is the specific gravity of the gas relative to air at 1 atm and 21.45 °C, P_o is the pressure downstream of the valve, and the expressions within the *min* function account for either non-choking or choking conditions. It is important to note that c_v in Eq. (14) is dimensionless when flow, pressure and temperature are expressed in units of SLPM, kPa and K, respectively. When concentrations, flows, temperatures, and the valve equation are not specified or required, consistency at the bed boundary is maintained by utilizing the corresponding balances given in Eqs. (4) to (6), and Eqs. (11) and (12), as shown in Table 1.

4 Bed, adsorbent and adsorbate characteristics

A summary of the bed, process and adsorbent characteristics, and equilibrium and kinetic information used in DAPS are tabulated in Table 2. The adsorbent was essentially the same NaX zeolite (i.e., 13X zeolite) used by Izumi et al. (2005). However, since no equilibrium adsorption isotherm data beyond the Henry's law region were available for CO isotope adsorption on 13X zeolite, equilibrium adsorption isotherms for ^{12}CO, ^{13}CO, and ^{14}CO were estimated from experimental results obtained for CO adsorption on 10X zeolite (Nolan et al. 1981), while keeping the same Henry's law constants for the CO isotopes on NaX zeolite reported by Izumi et al. (2005). Also, for a given isotherm, the maximum adsorbed phase loading was assumed to be the same for all three CO isotope species. The resulting hybrid 13X/10X zeolite equilibrium adsorption isotherms for ^{12}CO, ^{13}CO, and ^{14}CO are shown in Fig. 2 at three different temperatures. The single-gas Toth isotherm (Eqs. (5a), (5b) written for one species) was used to fit all the experimental data simultaneously; the resulting parameters are summarized in Table 2.

Since there was limited information available in the literature on the diffusion of CO isotopes in NaX zeolite, some assumptions were made on the mass transfer rates of

these species. Kärger et al. (1993) reported a very high mass transfer coefficient (>3.0 s^{-1}) for ^{13}CO in NaX zeolite at 227.6 K. Based on that study, the LDF mass transfer coefficient k_i was assumed to be the same for all the CO isotopes and equal to 1.0 s^{-1} for both adsorption and desorption.

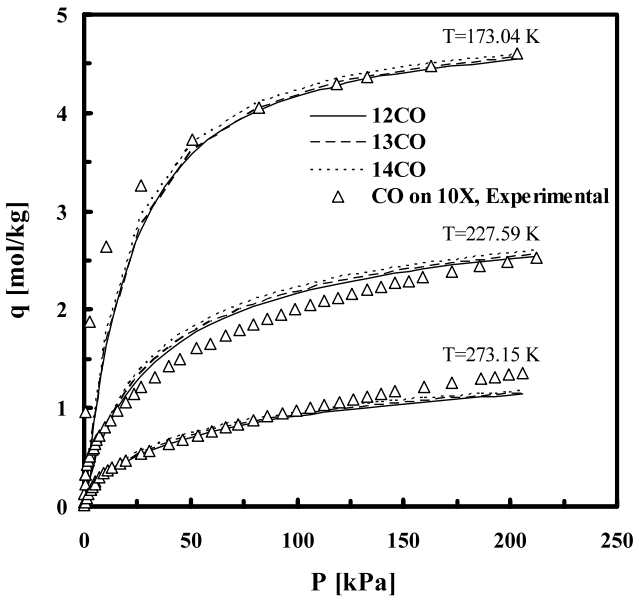

Fig. 2 Equilibrium adsorption isotherms for ^{12}CO, ^{13}CO and ^{14}CO on 13X/10X zeolite. The isotherms were created by combining the values of the Henry's law constants for CO isotopes on 13X zeolite from Izumi et al. (2005) with temperature dependent literature data for ^{12}CO on 10X zeolite, while keeping the maximum capacities at each of the three temperatures the same for each isotope. The *symbols* are experimental data from the literature and the *lines* are fits to the single-gas form of the Toth isotherm (Eq. (7))

5 Results and discussion

The results from 17 simulations of the three PSA cycles are provided in Table 3: five simulations of PSA Cycle I (total reflux with no ^{14}CO heavy product production), seven simulations of PSA Cycle II (discontinuous ^{14}CO heavy product production), and five simulations of PSA Cycle III (continuous ^{14}CO heavy product production). In all cases, the fresh feed composition was 1 ppm ^{14}CO and 1.9 mol% ^{13}CO in a balance of ^{12}CO; and the high pressure was $P_H = 120.0$ kPa, the low pressure was $P_L = 1.0$ kPa and the feed and wall temperatures were $T_F = T_W = 227.59$ K (Izumi et al. 2005). These and other conditions are shown in Table 2. The effects of the feed flow rate, cycle time t_{cyc}, CnD step valve coefficient c_v, and heavy reflux ratio R_R on the periodic state process performance in terms of the CO feed throughput (Eq. (3)), ^{14}CO enrichment (Eq. (1)) and ^{14}CO recovery (Eq. (2)) are tabulated in Table 3.

It must be emphasized that the separation factor, defined here as the ratio of the Henry's law constants for pairs of the ^{14}CO, ^{13}CO and ^{12}CO isotopes adsorbed by NaX zeolite, was indeed very small. Based on the numbers reported by Izumi et al. (2005) at the PSA cycle operating temperature (227.59 K) the separation factor for $^{14}CO/^{12}CO$ was 1.12 and that for $^{13}CO/^{12}CO$ was 1.05. Nevertheless, significant ^{14}CO enrichments were obtained by all three variants of the

Table 3 Parameter ranges investigated and PSA process performances in terms of the CO feed throughput, ^{14}CO recovery and ^{14}CO enrichment obtained with the 3-bed 3-step PSA cycles shown in Fig. 1

Run	PSA cycle[a]	Feed flow rate (SLPM)	Cycle time (s)	CnD valve coefficient (C_V)	Reflux ratio (R_R)	Throughput (L_{STP}/h/kg)	^{14}CO Enrichment	^{14}CO Recovery (%)
1	I	0.1000	7200	0.005	1.0000	1.968	98.45	0.00
2	I	0.1000	7200	0.010	1.0000	1.968	118.18	0.00
3	I	0.1000	7200	0.030	1.0000	1.968	152.64	0.00
4	I	0.1000	7200	0.050	1.0000	1.968	140.58	0.00
5	I	0.1000	7200	0.100	1.0000	1.968	65.28	0.00
6	II	0.0098	7200	0.030	0.9980	0.193	18.97	97.72
7	II	0.0245	7200	0.030	0.9950	0.482	18.11	91.76
8	II	0.0392	7200	0.030	0.9920	0.771	17.01	86.28
9	II	0.0489	7200	0.030	0.9900	0.962	16.35	82.92
10	II	0.0979	7200	0.030	0.9800	1.926	13.43	68.19
11	II	0.0196	3600	0.060	0.9980	0.386	19.51	96.12
12	II	0.0392	1800	0.120	0.9980	0.771	16.47	78.09
13	III	0.0098	7200	0.030	0.9996	0.193	19.10	98.61
14	III	0.0245	7200	0.030	0.9989	0.482	18.19	92.13
15	III	0.0392	7200	0.030	0.9982	0.771	17.08	86.51
16	III	0.0489	7200	0.030	0.9978	0.962	16.41	83.04
17	III	0.0979	7200	0.030	0.9956	1.926	13.47	68.22

[a]*PSA Cycle I*: total reflux; *PSA Cycle II*: discontinuous ^{14}CO production; *PSA Cycle III*: continuous ^{14}CO production

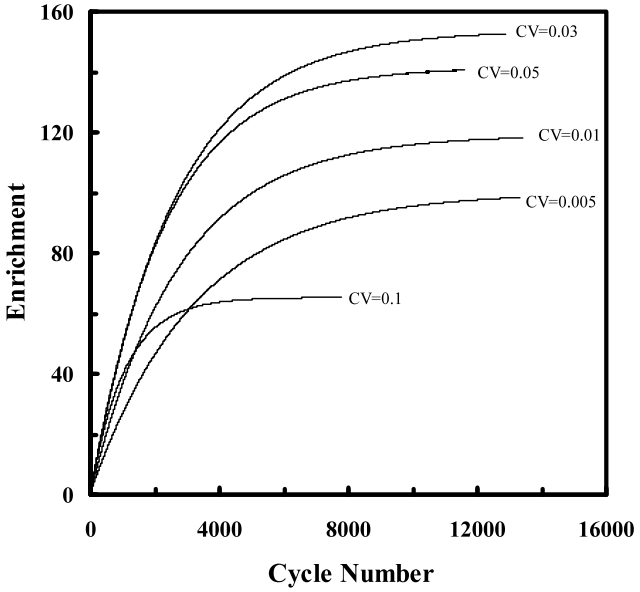

Fig. 3 Effect of the valve coefficient (c_v) on the average ^{14}CO enrichment in the bed during the approach to the periodic state while operating under total reflux (PSA Cycle I). The operating conditions for runs 1 to 5 are given in Table 3

3-bed 3-step PSA cycle proposed by Izumi et al. (2005), as shown in Table 3.

For PSA Cycle I ^{14}CO enrichments greater than 150 were readily obtained under total reflux. It is noteworthy that this total reflux PSA cycle represents the maximum possible ^{14}CO enrichment for a given set of PSA process conditions, just like in distillation. These enrichments were also boosted by the fact that this PSA cycle was operating under only a slight mass transfer limitation (very large $k_i = 1\ s^{-1}$). As an aside, much higher enrichments could be achieved with a more stringent set of PSA process conditions. In fact, intuition suggests that isothermal equilibrium theory would predict an unlimited enrichment of ^{14}CO using this 3-bed 3-step HR PSA cycle. Thus, in principle a ^{14}CO enrichment of 10^6 would produce a heavy product stream containing pure ^{14}CO. However, the practicality of doing so would be prohibitive because of the extremes in flow rates and high to low pressure ratios that would be required. Under more practical conditions, like those utilized in this study and by Izumi et al. (2005), the results in Table 3 show that ^{14}CO enrichments between 13 and 20 were easily achieved at very high ^{14}CO recoveries between 68 and 99 % when a ^{14}CO product was produced using PSA Cycle II or III. The factors that were found to affect the magnitude of the ^{14}CO enrichment and ^{14}CO recovery are presented in Figs. 3 to 8 and discussed below.

Figure 3 shows the effect of the CnD valve coefficient c_v, i.e., the effect of the countercurrent depressurization rate during the CnD step, on the ^{14}CO enrichment for PSA Cycle I (total reflux case with no ^{14}CO production). The results

Table 4 Final absolute pressure reached at the end of the countercurrent depressurization (CnD) step for different values of the valve coefficient (c_v)

c_v	P_L at End of CnD (kPa)
0.005	11.8
0.010	2.9
0.030	1.0
0.050	1.0
0.100	1.0

correspond to runs 1 to 5 in Table 3 for an arbitrary feed flow of 0.1 SLPM. The beds initially contained no ^{14}CO, 98 mol% ^{12}CO and 2 mol% ^{13}CO. For each c_v, the average ^{14}CO enrichment of the total gas leaving the heavy product end of the bed during the CnD step increased with cycle number, as the concentration of ^{14}CO in the bed slowly built up in time during the approach to the periodic state. The build-up continued until some of the ^{14}CO reached the light product end of the bed and began exiting the bed in the light product stream. The onset of ^{14}CO breakthrough in the light product was revealed by the average ^{14}CO concentration (enrichment) leaving the CnD step eventually exhibiting a plateau, which also indicated the periodic state was attained. Between 8,000 and 14,000 cycles were required to reach the periodic state, depending on the PSA cycle and conditions. Also, the ^{14}CO enrichment exhibited a maximum for $c_v = 0.03$. This maximum occurred for the following reasons.

At a small c_v the ^{14}CO enrichment was low because the valve was not opened enough to achieve the desired low pressure of 1.0 kPa by the end of the CnD step. Table 4 lists the values of the low pressure (P_L) achieved by the end of the CnD step for different values of the c_v. A $c_v = 0.03$ or greater was required. The inability to reach P_L limited desorption of any of the CO species, which, in turn, reduced the ^{14}CO enrichment. In contrast, at a large c_v the higher flow rate during the CnD step caused the ^{14}CO mass transfer zone (MTZ) in the bed to broaden during both the HR and FP/F steps. Recall that while the CnD step provided the gas for the HR step, the light product from the HR step simultaneously provided the gas for the FP/F step initially at a much lower pressure and thus at very high velocities. These high velocities broadened the MTZ, which caused the ^{14}CO to be more dispersed in the bed, which, in turn, reduced its enrichment. Breakthrough curves are provided later that substantiate this counterintuitive assertion of a mass transfer limitation in a PSA cycle operated with such a large mass transfer coefficient (i.e., $k_i = 1\ s^{-1}$).

The outcome of this mass transfer limitation was that at some intermediate c_v, in this case $c_v = 0.03$, the ^{14}CO enrichment exhibited a maximum, indicating that an optimum countercurrent depressurization rate existed during the CnD

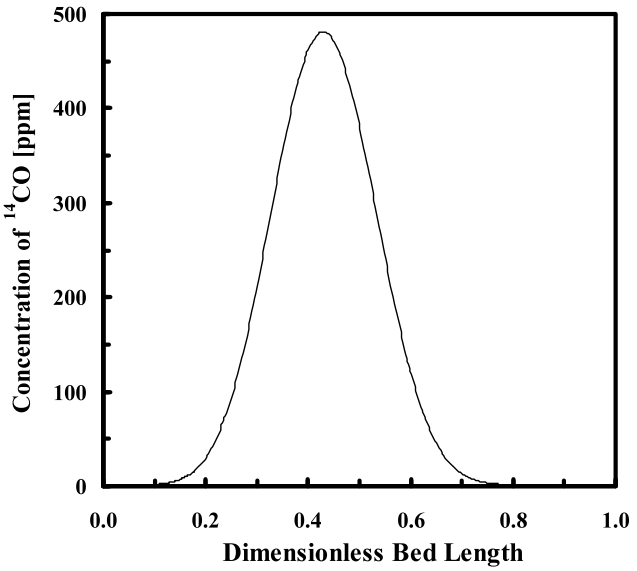

Fig. 4 ^{14}CO gas phase concentration profile in the bed at the end of the HR step for $c_v = 0.03$. The operating conditions for run 3 are given in Table 3

step. Thus, $c_v = 0.03$ was used in all subsequent runs for which the cycle time t_{cyc} was 7200 s. To stay at this optimum condition for other t_{cyc} the c_v was scaled according to the following formula:

$$c_v = 0.03\left(\frac{7200}{t_{cyc}(s)}\right) \tag{15}$$

Figure 4 shows the periodic state gas phase concentration profile in the bed at the end of the HR step for run 3 (PSA Cycle I). Notice the conspicuous bell-shaped curve. Although ^{14}CO was breaking through the light product end of the bed during the HR step, its enrichment along the bed was so significant (maximum concentration of about 493 ppm) that the ^{14}CO gas phase concentrations at either end of the bed were not perceivable in this plot. Indeed, this bell-shaped curve was a direct consequence of the bell-shaped concentration profile leaving the heavy product end of the bed during the CnD step. This effluent profile is shown in Fig. 5, along with the corresponding variation of the pressure in the bed during the CnD step. As the pressure decreased, the effluent concentration profile went through a sharp maximum, with an instantaneous ^{14}CO concentration of just over 500 ppm and an average ^{14}CO concentration of over 153 ppm (i.e., enrichment of 153). Although these results were attained under total reflux with no heavy product production, they alluded to the possibility of achieving significant ^{14}CO enrichments even under finite reflux with heavy product production, as done with PSA Cycles II and III.

It was also clear from Fig. 5a that most of the ^{14}CO exited the bed between 50 and 600 s into the CnD step, while practically no ^{14}CO enrichment was observed after 700 s into the

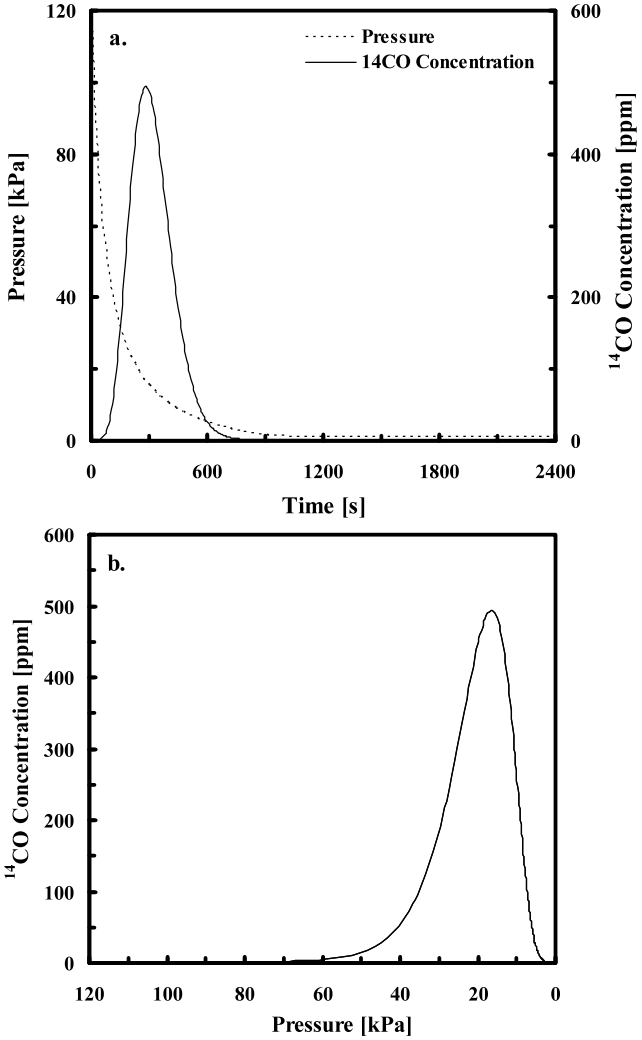

Fig. 5 (**a**) ^{14}CO concentration (or enrichment) exiting the bed during the CnD step and corresponding pressure history. (**b**) ^{14}CO concentration (or enrichment) exiting the bed during the CnD step as a function of the CnD pressure history for $c_v = 0.03$. The operating conditions for run 3 are given in Table 3

CnD step. The presence of a bell-shaped curve during the CnD step of essentially any PSA cycle instilled Yamaho et al. (1987) to divide the CnD step into three different stages, i.e., initial, middle and final stages, in an attempt to further concentrate the heavy component. Heavy product production occurred only during some arbitrary time interval in the middle of the CnD step where the concentration was highest. PSA Cycle II, with discontinuous ^{14}CO heavy product production, was based on this approach. The results are tabulated in Table 3, runs 6 to 12.

It was apparent from the curves in Fig. 5 that for run 3 an adequate time for ^{14}CO heavy product production would have been the period between 200 and 400 s into the CnD step. This period was equivalent to 1/12 of the CnD step duration beginning at 1/12 elapsed time into the CnD step. Considering that the c_v of the CnD step was adjusted as

inversely proportional to t_{cyc} (Eq. (15)), which necessarily forced all the concentration profiles to be identical relative to the step time, it was expected that the location and duration of the production (middle) stage would also remain the same relative to the step time. Furthermore, it was envisioned that the relative shape of the curve in Fig. 5 would not change in going from a total reflux mode to a production mode. Consequently, for PSA Cycle II (with discontinuous ^{14}CO heavy product production) the durations of the three stages of the CnD step were chosen as follows: The duration of the initial stage, with a $R_R = 1$, was equal to $1/12$ of the CnD step. The middle stage, with $R_R < 1$, was also equal to $1/12$ of the CnD step. The final stage, with a $R_R = 1$, was equal to $10/12$ of the CnD step, i.e., the remainder of the CnD step. The results for PSA Cycle II are tabulated in Table 3, runs 6 to 12. In contrast, PSA Cycle III was operated with $R_R < 1$ and thus with continuous ^{14}CO heavy product production during the entire CnD step.

Figure 6a displays the effect of the CO feed throughput on the ^{14}CO enrichment and ^{14}CO recovery for both PSA Cycles II (discontinuous ^{14}CO production, runs 6 to 10, Table 3) and III (continuous ^{14}CO production, runs 13 to 17, Table 3) for $t_{cyc} = 7200$ s. The fresh feed flow rate (F) into the bed during the F/FP step was not independently defined, but instead evaluated according to the following heuristic expression:

$$F = 20(1 - R_R) \times \frac{\text{total moles CO obtained as product during CnD step}}{(\text{mass adsorbent in one bed})(\text{feed step time})} \quad (16)$$

Equation (16) assumes an ideal separation situation, where ^{14}CO is enriched 20 times (hence, the 20 in Eq. (16)) by recovering 100 % of it. As a result, F (and thus, the CO feed throughput) was determined simply by defining the value for the heavy reflux ratio R_R. The relationship between R_R and the CO feed throughput (or F) is shown in Fig. 6b. Using the heuristic approach defined by Eq. (16), ^{14}CO recoveries of over 95 % with ^{14}CO enrichments of over 15 were readily achieved. In fact, extrapolation of the curves in Fig. 6a resulted in the expected limit corresponding to a ^{14}CO recovery of 100 % and a ^{14}CO enrichment of 20. These results clearly indicated that there is no limit to the ^{14}CO purities and ^{14}CO recoveries that could be achieved with this 3-bed 3-step PSA process, regardless of the low separation factor between the species involved. This interesting summation was inferred earlier based on equilibrium theory. The only requirement is a specification of the desired enrichment from Eq. (16). Of course, high ^{14}CO enrichments and high ^{14}CO recoveries would come at a cost, namely, very low CO feed throughputs and very high heavy reflux ratios (>0.995), resulting respectively in both high capital and operating (i.e., recompression) costs.

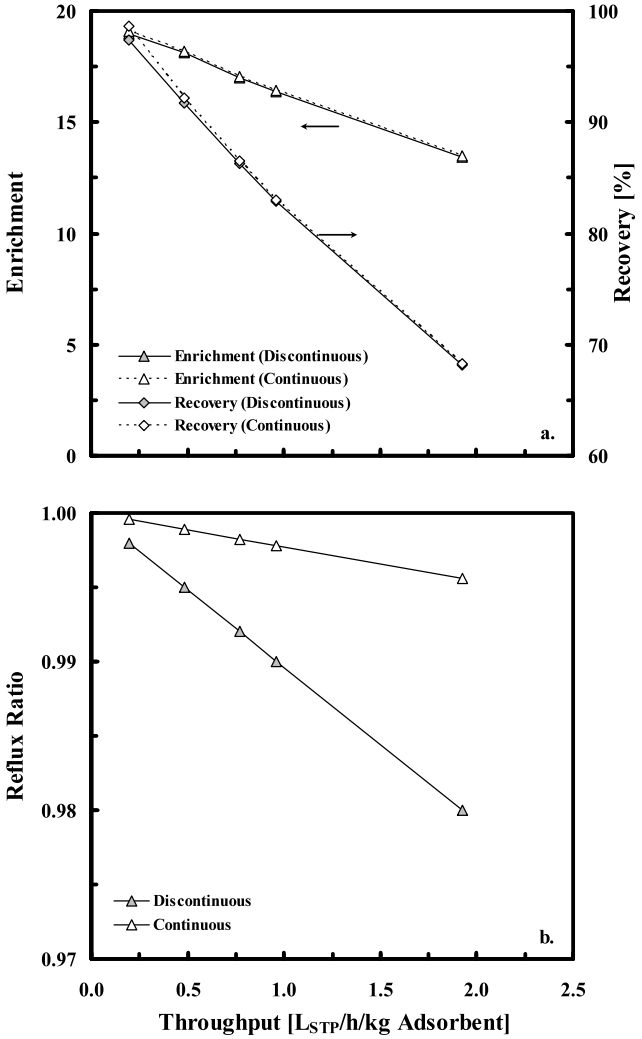

Fig. 6 (**a**) Effect of the CO feed throughput (and thus reflux ratio (R_R) via Eq. (16)) on the ^{14}CO enrichment and ^{14}CO recovery for $t_{cyc} = 7200$ s. (**b**) Relationship between R_R and CO feed throughput (Eq. (16)) for 200 s (discontinuous) and 2400 s (continuous) product withdrawal durations during the CnD step. The operating conditions for PSA Cycle II (discontinuous, runs 6 to 10), and those for PSA Cycle III (continuous, runs 13 to 17), are given in Table 3

The results in Fig. 6a also showed essentially no difference in the performance between PSA Cycle II (discontinuous ^{14}CO production) and PSA Cycle III (continuous ^{14}CO production). This was a surprising and counterintuitive result that deserves further explanation, especially since the discontinuous PSA Cycle II approach was highly touted in the literature as a means to further concentrate the heavy component from a dilute feed stream (Yamaho et al. 1987). Recall that both PSA cycles used the same cycle time, high to low pressure ratio, and feed flow rate determined from Eq. (16). The reflux ratios (Table 3) were necessarily different to accommodate the discontinuous and continuous versions of the PSA cycles. Equation (16) also a priori adjusted the conditions to achieve a specified ideal performance cor-

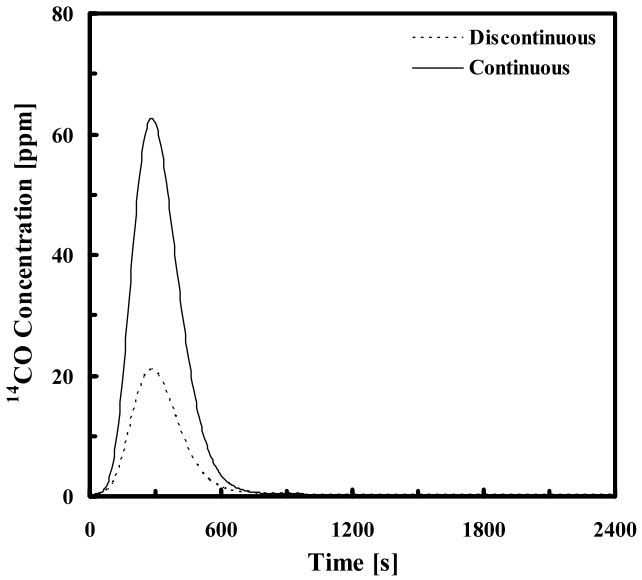

Fig. 7 ^{14}CO concentration exiting the bed during the CnD step for the discontinuous (II) and continuous (III) PSA cycles with the same feed flow rate, i.e., runs 7 and 14, respectively. The operating conditions are given in Table 3

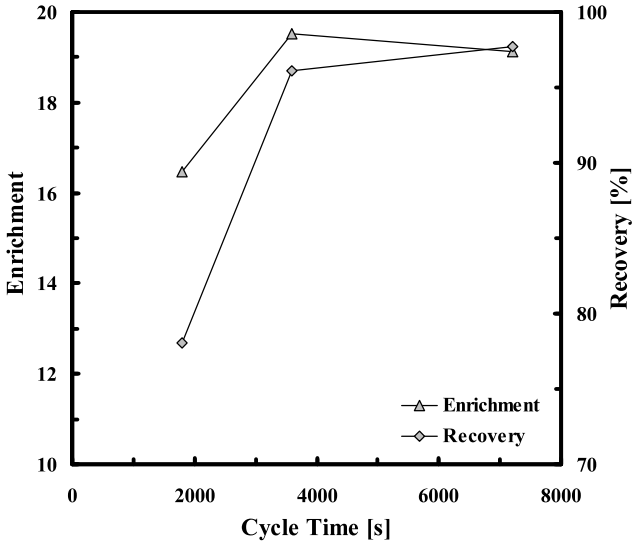

Fig. 8 Effect of the cycle time t_{cyc} on the ^{14}CO enrichment and ^{14}CO recovery at $R_R = 0.998$. The operating conditions for runs 6, 11 and 12 are given in Table 3

responding to a ^{14}CO enrichment of 20 and a ^{14}CO recovery of 100 %. Now, consider the following facts for both PSA cycles. The total amount of CO leaving the column during the CnD step was invariant, as it depended only on the high to low pressure ratio. Only a minute amount of heavy product gas was ever withdrawn from the CnD step in each case, making both reflux ratios were very close to unity (Table 3). The ^{14}CO effluent concentration profiles shown in Fig. 7 (runs 7 and 14 in Table 3) both exited the bed early during the CnD step, indicating they were both located close to the heavy product end of the bed at the end of the HR step and that the gas leaving the light product end of the bed during the HR step was essentially invariant. The light product produced during the F/FP step was also invariant, as the entire CO exiting the light product end of the bed during the HR step was recycled to the F/FP step. Under these circumstances, a simple mass balance demanded that the ^{14}CO enrichment and ^{14}CO recovery be the same for both PSA cycles. Hence, for this very dilute system that demanded a good performance, there was no benefit of implementing the more complex discontinuous approach of Yamaho et al. (1987) that supposedly took advantage of selectively removing only the highest concentrations from the ^{14}CO bell-shaped concentration profile that developed in the bed during the CnD step (Figs. 5 and 7).

It was also interesting that the bell-shaped effluent concentration profile for PSA Cycle II (discontinuous ^{14}CO product production) was significantly smaller than that for PSA Cycle III (continuous ^{14}CO product production), as shown in Fig. 7. This was a consequence of removing the highest ^{14}CO concentrations from the bed during the middle of the CnD step and refluxing less. Since less ^{14}CO was sent back to the bed undergoing the HR step, the ^{14}CO concentration did not build up as much in the bed. Nevertheless, based on the aforementioned arguments that explained why both PSA cycles resulted in the same performance, it did not matter whether the high ^{14}CO concentrations were taken as product and the low ^{14}CO concentrations were used as reflux in a discontinuous mode during the CnD step (PSA Cycle II), or whether all the ^{14}CO concentrations were taken as product in a continuous mode with them varying from low to high to low during the CnD step (PSA Cycle III). In the end, for this very dilute feed stream, a priori demanding a stringent performance on the heavy product enrichment and recovery resulted in nearly identical PSA process performances, thereby making the continuous and simpler operational mode for removing a minute amount of heavy product gas from the bed during the CnD step the logical choice.

Figure 8 shows the effect of the cycle time t_{cyc} on the PSA process performance. The results correspond to runs 6, 11 and 12 in Table 3 (i.e., PSA Cycle II). The same results would be obtained for PSA Cycle III, as noted above. The feed flow rates were also defined according to Eq. (16) and increased inversely proportional to t_{cyc}. Consequently, the fresh feed F fed into a bed during the FP/P step remained constant, although the CO feed throughput increased with t_{cyc} decreasing. Reducing t_{cyc} to increase the CO feed throughput resulted in a significant deterioration of the PSA process performance. For example, decreasing the cycle time by a factor of four from 7200 to 1800 s, caused the ^{14}CO enrichment and ^{14}CO recovery to both plummet from

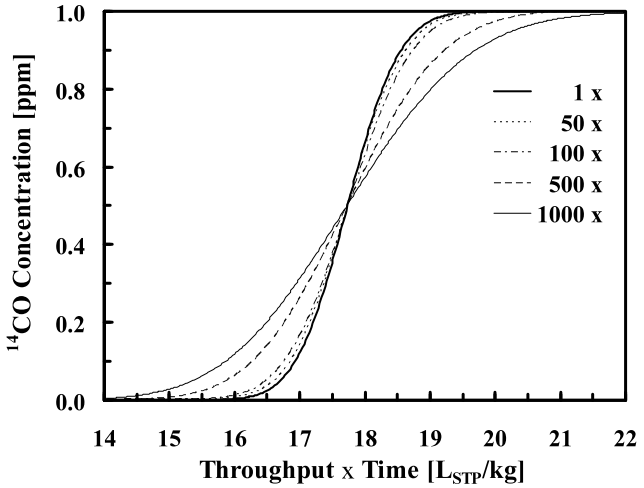

Fig. 9 Breakthrough curves at 227.59 K and 120 kPa for different feed flow rates for the CO isotope feed concentration provided in Table 2 with the initial state of the bed in equilibrium with 2 % ^{13}CO and 98 % ^{12}CO and no ^{14}CO. The feed flow rate is indicated in multiples of the base case feed flow rate corresponding to run 6 in Table 3. The abscissa is expressed in terms of the corresponding feed throughput times the elapsed time

18.97 to 13.43 and from 97.72 to 68.19 %, respectively. This indicated that despite the relatively large mass transfer coefficient that was used for all three isotopes, i.e., $k_i = 1\ s^{-1}$, the process was indeed mass transfer limited.

As with the role of the c_v discussed earlier (Fig. 3), this mass transfer limitation was caused by the large velocities associated with the flow into the FP/F step that came from the recycled (Rec) light product flow from the HR step (see Fig. 1). For run 6 in Table 3, the resulting interstitial velocities during the pressurization portion of the FP/F step exhibited a maximum of around 2.5 m/s (not shown) when the bed pressure was still under vacuum, i.e., 10 kPa. This maximum velocity was more than 1000 times larger than the interstitial velocity of 0.0022 m/s (not shown) contributed by just the feed.

To show the role of the flow rate on the mass transfer of ^{14}CO, Fig. 9 displays breakthrough curves for different feed flow rates into a single bed at 120 kPa and 227.59 K using the same feed concentration as in the PSA process. The base case flow rate was based on the feed flow rate of run 6 in Table 3, which was 0.0098 SLPM. The elapsed time is expressed in terms of the feed throughput times the elapsed time. It is clear that when the flow rate was increased to about 100 times that of the feed flow rate of run 6, the breakthrough curves did not overlap anymore, indicating that the process was becoming more mass transfer limited. When the flow rates were less than 100 times that of the feed flow rate of run 6, the bed was practically under local equilibrium, with the observed dispersion in Fig. 9 caused by numerical dispersion. When the flow rate was increased 1000 times, the effect of flow rate on the mass transfer process was even more apparent. These breakthrough results explained very well how the PSA process became mass transfer limited. It was due to the very large pressurization flows experienced during the FP/F step, particularly when t_{cyc} was decreased from 7200 to 1800 s. It also became apparent that such a PSA process would, in fact, always be limited to very low CO feed throughputs, especially if high ^{14}CO enrichments and high ^{14}CO recoveries are desired.

6 Conclusions

Simulations of three different 3-bed 3-step PSA cycles were carried out to study the enrichment and recovery of ^{14}CO from an isotopic mixture of ^{14}CO, ^{13}CO and ^{12}CO using NaX zeolite. Each PSA cycle included feed pressurization/feed (FP/P), heavy reflux (HR) and countercurrent depressurization (CnD) steps; they differed only in the way the CnD step was carried out. PSA Cycle I was carried out under total reflux (i.e., with no ^{14}CO heavy product production). This case represented the best possible ^{14}CO enrichment for a given set of process conditions, just like in distillation. PSA Cycle II was carried out with discontinuous ^{14}CO heavy product production. In this PSA cycle, ^{14}CO product production occurred only during the middle stage (0/12 to 1/12 time step interval) of the CnD step under finite heavy reflux, with total heavy reflux being used during the initial stage (1/12 to 2/12 time step interval) and final stage (2/12 to 12/12 time step interval) of the CnD step. This operational mode was done in an attempt to further enrich ^{14}CO by selectively removing only the highest ^{14}CO concentrations from the CnD step. PSA Cycle III was carried out with continuous ^{14}CO heavy product production, i.e., with finite heavy reflux being used during the entire CnD step. This was the more conventional operational mode. For these 3-bed 3-step PSA cycles, the effects of the CnD step valve coefficient (c_v), heavy reflux ratio (R_R), and cycle time (t_{cyc}) on the PSA process performance were determined in terms of the ^{14}CO enrichment, ^{14}CO recovery and CO feed throughput. Three key conclusions were drawn from this study.

There was essentially no limit to the extent of the ^{14}CO enrichment that could be achieved, despite the inherently low ^{14}CO/^{12}CO (1.05) and ^{14}CO/^{13}CO (1.12) separation factors for these isotopes on NaX zeolite. Under total reflux (PSA Cycle I) an optimum c_v was found for the CnD step and ^{14}CO enrichments as high as 152 were obtained. Using the optimum c_v under finite reflux a ^{14}CO enrichment approaching 20 and a ^{14}CO recovery approaching 100 % were easily achieved with discontinuous (PSA Cycle II) or continuous (PSA Cycle III) ^{14}CO heavy product production. However, such an isotope separation process comes at the expense of elevated capital and operating costs, as revealed by the low CO feed throughputs and very high heavy reflux

ratios required. The ^{14}CO enrichment and the ^{14}CO recovery both increased with decreasing CO feed throughputs and higher R_R, which were always very close to unity.

The results also revealed that despite the relatively high mass transfer coefficient used by all three isotopes ($k_i = 1\ s^{-1}$), the PSA cycle exhibited a mass transfer limitation. This mass transfer limitation caused the ^{14}CO enrichment and ^{14}CO recovery to both plummet from 18.97 to 13.43 and from 97.72 to 68.19 %, respectively when the cycle time t_{cyc} was decreased from 7200 to 1800 s. This mass transfer limitation was caused by the high flow leaving the CnD step and large heavy reflux ratio that led to large velocities into the FP/F step through the recycled (Rec) light product flow from the HR step. Although these rather long cycle times would, by no means, be considered rapid PSA, a decrease in t_{cyc} significantly limited the possibility of improving the CO feed throughput without compromising both the ^{14}CO enrichment and ^{14}CO recovery.

Finally, there was essentially no difference in the performance of PSA Cycles II and III when operating under the same process conditions, a counterintuitive result. However, it was determined that because only traces of ^{14}CO were removed as heavy product, the reflux ratios were very large, and the ^{14}CO concentration in the light product was essentially invariant, a mass balance demanded that the performances of PSA Cycles II and III be the same. It did not matter whether the high ^{14}CO concentrations were taken as product and low ^{14}CO concentrations were used as reflux in a discontinuous mode during the CnD step (PSA Cycle II), or whether all ^{14}CO concentrations were taken as product in a continuous mode with them varying from low to high to low during the CnD step (PSA Cycle III). In the end, for a very dilute feed and by a priori demanding a reasonably good PSA process performance, nearly identical PSA process performances were achieved, making the continuous and simpler operational mode for removing a minute amount of concentrated heavy product from the bed during the CnD step the logical choice.

Acknowledgement The authors gratefully acknowledge financial support provided by Studsvik, Inc.

References

Fachinger, J., von Lensa, W., Podruhzina, T.: Decontamination of nuclear waste. Nucl. Eng. Des. **238**, 3086–3091 (2008)

Izumi, J., Yasutake, A., Kobayashi, S., Shikichi, A., Kinugasa, A., Kohanawa, O., Okumara, M., Kanda, T., Izumoji, Y., Saigusa, M., Oguri, D., Inoue, T., Oumori, S.: ^{14}CO and ^{12}CO separation on Na-X using pressure swing adsorption at low temperatures. Adsorption **11**, 817–821 (2005)

Jaroniec, M., Toth, J.: Adsorption of gases on heterogeneous solid surfaces: I. Extension of Toth isotherm on adsorption from gas mixtures. Colloid Polym. Sci. **254**, 643–649 (1976)

Kärger, J., Pfeifer, H., Stallmach, F., Feoktistova, N.N., Zhdanov, S.P.: ^{129}Xe and ^{13}C PFG n.m.r. study of the intracrystalline self-diffusion of Xe, CO_2 and CO. Zeolites **13**, 50–55 (1993)

Nolan, I.T., McKeehan, T.W., Danner, R.P.: Equilibrium adsorption of oxygen, nitrogen, carbon monoxide, and their binary mixtures on molecular sieve type 10X. J. Chem. Eng. Data **26**, 112–115 (1981)

Reynolds, S.P., Ebner, A.D., Ritter, J.A.: Stripping PSA cycles for CO_2 recovery from flue gas at high temperature using a hydrotalcite-like adsorbent. Ind. Eng. Chem. Res. **45**, 4278–4294 (2006)

Yamaho, M., Aono, T., Kurimoto, M., Uno, M.: Process for separation of high purity gas from mixed gas. WO 87/01611, PCT/JP86/00465 (1987)